AFRL-AFOSR-VA-TR-2016-0031

Investigation of 3D Shock-Boundary Layer Interaction A Combined Approach using Experiments, Numerical Simulations and Stability Analysis

Jesse Little
ARIZONA UNIV BOARD OF REGENTS TUCSON

12/02/2015
Final Report

Air Force Research Laboratory
AF Office Of Scientific Research (AFOSR)/ RTA1
Arlington, Virginia 22203
Air Force Materiel Command

REPORT DOCUMENTATION PAGE

Form Approved
OMB No. 0704-0188

PLEASE DO NOT RETURN YOUR FORM TO THE ABOVE ORGANIZATION.

1. REPORT DATE *(DD-MM-YYYY)*	2. REPORT TYPE	3. DATES COVERED *(From - To)*
11-22-2015	FINAL PERFORMANCE REPORT	15 July 2014 to 14 July 2015

4. TITLE AND SUBTITLE
Investigation of 3D Shock-Boundary Layer Interaction: A Combined Approach using Experiments, Numerical Simulations and Stability Analysis

5a. CONTRACT NUMBER

5b. GRANT NUMBER
FA9550-14-1-0195

5c. PROGRAM ELEMENT NUMBER

6. AUTHOR(S)
Little, Jesse
Fasel, Hermann

5d. PROJECT NUMBER

5e. TASK NUMBER

5f. WORK UNIT NUMBER

7. PERFORMING ORGANIZATION NAME(S) AND ADDRESS(ES)
UNIVERSITY OF ARIZONA
888 N EUCLID AVE
TUCSON AZ 85719-4824

8. PERFORMING ORGANIZATION REPORT NUMBER
3010480

9. SPONSORING/MONITORING AGENCY NAME(S) AND ADDRESS(ES)
USAF, AFRL DUNS 143574726
AF OFFICE OF SCIENTIFIC RESEARCH
875 N. RANDOLPH ST. ROOM 3112
ARLINGTON VA 22203

10. SPONSOR/MONITOR'S ACRONYM(S)

11. SPONSOR/MONITOR'S REPORT NUMBER(S)

12. DISTRIBUTION/AVAILABILITY STATEMENT
DISTRIBUTION A. Approved for public release.

13. SUPPLEMENTARY NOTES

14. ABSTRACT

The characteristics of impinging oblique shock turbulent boundary layer interaction (SBLI) are examined using experiments, simulations and stability analysis. The experimental focus is on application of stereoscopic particle image velocimetry (PIV) to the flow field produced by an impinging shock (produced by a 15 degree wedge) that is swept at angles of 0, 22.5, and 40 degrees in Mach 2.3 flow. The interaction length is found to decrease with increasing sweep angle across the test matrix. The 22.5 degree and unswept case have cylindrical similarity and the 40 degree interaction appears conical. All cases show separated flow in the interaction region and most contain reverse flow that is clearly outside of the measurement uncertainty. A corresponding numerical SBLI study is undertaken for a laminar approach boundary layer at Mach 2.0. The skin friction and pressure distribution from the simulations are compared to experimental measurements and numerical results available in the literature. The response to low–amplitude disturbances is investigated in order to study the linear stability behavior of the separation bubble. The effects of the shock incidence angle and Reynolds number are also investigated. Three–dimensional simulations are performed in order to explore transition.

15. SUBJECT TERMS

16. SECURITY CLASSIFICATION OF:			17. LIMITATION OF ABSTRACT	18. NUMBER OF PAGES	19a. NAME OF RESPONSIBLE PERSON
a. REPORT	b. ABSTRACT	c. THIS PAGE		24	Jesse Little, PhD
					19b. TELEPHONE NUMBER *(Include area code)* 520-626-8677

Reset

INSTRUCTIONS FOR COMPLETING SF 298

1. REPORT DATE. Full publication date, including day, month, if available. Must cite at least the year and be Year 2000 compliant, e.g. 30-06-1998; xx-06-1998; xx-xx-1998.

2. REPORT TYPE. State the type of report, such as final, technical, interim, memorandum, master's thesis, progress, quarterly, research, special, group study, etc.

3. DATES COVERED. Indicate the time during which the work was performed and the report was written, e.g., Jun 1997 - Jun 1998; 1-10 Jun 1996; May - Nov 1998; Nov 1998.

4. TITLE. Enter title and subtitle with volume number and part number, if applicable. On classified documents, enter the title classification in parentheses.

5a. CONTRACT NUMBER. Enter all contract numbers as they appear in the report, e.g. F33615-86-C-5169.

5b. GRANT NUMBER. Enter all grant numbers as they appear in the report, e.g. AFOSR-82-1234.

5c. PROGRAM ELEMENT NUMBER. Enter all program element numbers as they appear in the report, e.g. 61101A.

5d. PROJECT NUMBER. Enter all project numbers as they appear in the report, e.g. 1F665702D1257; ILIR.

5e. TASK NUMBER. Enter all task numbers as they appear in the report, e.g. 05; RF0330201; T4112.

5f. WORK UNIT NUMBER. Enter all work unit numbers as they appear in the report, e.g. 001; AFAPL30480105.

6. AUTHOR(S). Enter name(s) of person(s) responsible for writing the report, performing the research, or credited with the content of the report. The form of entry is the last name, first name, middle initial, and additional qualifiers separated by commas, e.g. Smith, Richard, J, Jr.

7. PERFORMING ORGANIZATION NAME(S) AND ADDRESS(ES). Self-explanatory.

8. PERFORMING ORGANIZATION REPORT NUMBER. Enter all unique alphanumeric report numbers assigned by the performing organization, e.g. BRL-1234; AFWL-TR-85-4017-Vol-21-PT-2.

9. SPONSORING/MONITORING AGENCY NAME(S) AND ADDRESS(ES). Enter the name and address of the organization(s) financially responsible for and monitoring the work.

10. SPONSOR/MONITOR'S ACRONYM(S). Enter, if available, e.g. BRL, ARDEC, NADC.

11. SPONSOR/MONITOR'S REPORT NUMBER(S). Enter report number as assigned by the sponsoring/ monitoring agency, if available, e.g. BRL-TR-829; -215.

12. DISTRIBUTION/AVAILABILITY STATEMENT. Use agency-mandated availability statements to indicate the public availability or distribution limitations of the report. If additional limitations/ restrictions or special markings are indicated, follow agency authorization procedures, e.g. RD/FRD, PROPIN, ITAR, etc. Include copyright information.

13. SUPPLEMENTARY NOTES. Enter information not included elsewhere such as: prepared in cooperation with; translation of; report supersedes; old edition number, etc.

14. ABSTRACT. A brief (approximately 200 words) factual summary of the most significant information.

15. SUBJECT TERMS. Key words or phrases identifying major concepts in the report.

16. SECURITY CLASSIFICATION. Enter security classification in accordance with security classification regulations, e.g. U, C, S, etc. If this form contains classified information, stamp classification level on the top and bottom of this page.

17. LIMITATION OF ABSTRACT. This block must be completed to assign a distribution limitation to the abstract. Enter UU (Unclassified Unlimited) or SAR (Same as Report). An entry in this block is necessary if the abstract is to be limited.

Final Report

Investigation of 3D Shock-Boundary Layer Interaction: A Combined Approach using Experiments, Numerical Simulations and Stability Analysis

Air Force Office of Scientific Research
Contract Number: FA9550-14-1-0195
Program Manager: Dr. Ivett Leyva

Jesse Little (PI), Hermann Fasel, Andreas Gross
Department of Aerospace and Mechanical Engineering
University of Arizona

November 2015

I. Abstract

The characteristics of unswept and swept impinging oblique shock turbulent boundary layer interaction (SBLI) are examined using experiments, simulations and stability analysis. The experimental focus is on application of stereoscopic particle image velocimetry (PIV) to the flow field produced by an impinging shock (produced by a 15 degree wedge) that is swept at angles of 0, 22.5, and 40 degrees in Mach 2.3 flow. The SBLI is investigated at three spanwise planes. The interaction length is found to decrease with increasing sweep angle across the test matrix. The 22.5 degree and unswept case have cylindrical similarity and the 40 degree interaction appears conical. The present study also includes a mirrored 40 degree swept case, which shows that the results are not due to a particular sidewall boundary layer. All cases show separated flow in the interaction region and most contain reverse flow that is clearly outside of the measurement uncertainty. A corresponding numerical SBLI study is undertaken for a laminar approach boundary layer at Mach 2.0. The numerical conditions are chosen for modification and validation of an existing in-house code. The skin friction and pressure distribution from the simulations are compared to experimental measurements and numerical results available in the literature. Results confirm the asymmetric nature of the separation bubble as reported in the classical literature. In addition to the steady flow field calculations, the response to low–amplitude disturbances is investigated in order to study the linear stability behavior of the separation bubble. For comparison, both the development of two–dimensional and three–dimensional (oblique) disturbances are studied with and without the impinging oblique shock. Furthermore, the effects of the shock incidence angle and Reynolds number are investigated. Three–dimensional direct numerical simulations are performed in order to explore the laminar-turbulent transition process in the presence of a laminar separation bubble generated by an impinging shock. The results presented here summarize efforts during a one-year seed grant and show that the necessary tools for linking experiments and computations have been developed. A major focus of future efforts is to more closely link the research tracks.

II. Table of Contents

III. Introduction

Shock-wave boundary layer interactions (SBLIs) occur in most supersonic flight applications and have been the subject of many studies since the mid-20th century when research began on transonic flows. Due to renewed interest in sustained high-speed atmospheric flight, they are again receiving considerable attention. The general characteristics of these interactions are well-known and well-documented. An obstruction in the boundary layer (compression corner, impinging shock, fin, or other shock generator) creates a region of thickened or separated boundary layer flow. An oblique shock is formed upstream of the interaction, where the freestream perceives the thickened viscous region much like an obstacle (Figure 1). SBLIs are unsteady and the thickened or separated region grows/shrinks over time, moving the shock along with it. This unsteadiness is known to occur at both low and high frequencies (Figure 1). Particular focus has been placed on identifying the source of the low frequency unsteadiness for both scientific and practical reasons. In practical applications the low-frequency unsteadiness can affect the performance of air-breathing propulsion systems or couple with the structural dynamics of control surfaces. In these instances, in-flight structural fatigue loading and catastrophic loss of the vehicle may occur. The frequency associated with this unsteadiness is one to three orders of magnitude lower than the characteristic frequency of the incoming boundary layer. A comprehensive introduction into SBLI of various kinds can be found, for example, in the review paper by Dolling.[1] According to Dolling, important quantities like peak heating in strong interactions and unsteady pressure peaks still cannot be predicted very accurately or even not at all, especially for complex geometries and flow fields.

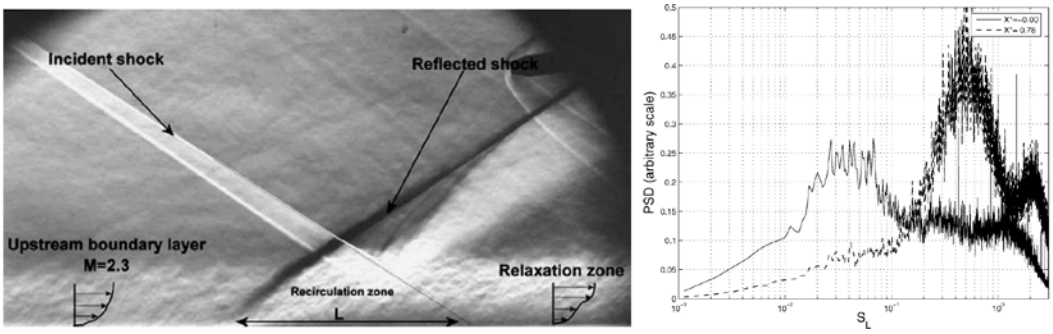

Figure 1: Schlieren image of incident SBLI (left) and pressure spectra at two streamwise locations in recirculation region (right).[2]

The fundamental flow physics behind the low frequency oscillations are still unclear and the subject of ongoing research, but much has been discovered. Many experimental studies have suggested that the low-frequency unsteadiness is correlated to streaks in the incoming turbulent boundary layer.[3-6] These streaks occur at a broadband frequency, but they can force the low frequency motion. Plotkin proposed a low-order stochastic SBLI model which was later validated in part by Poggie and Smits (2001 and 2005).[7-9] Touber and Sandham (2011) refined the model and showed that it played the role of a low-pass filter, so that the low-frequency unsteadiness may simply be interpreted as the system response to white noise.[10] Others suggest that the unsteadiness arises from the dynamics of the separation bubble itself.[2,11-13] A large-eddy simulation (LES) by Touber and Sandham showed that coherent structures in the incoming boundary layer are not a prerequisite for low-frequency unsteadiness.[14] They state however, that the streaks could excite intrinsic SBLI dynamics resulting in the behavior observed by Ganapathisubramani et al.[3,4] and Humble et al.[5,6] More recently Clemens et al. documented that SBLI studies (primarily on compression ramps) showing the most influence from the upstream boundary layer tended to have unseparated or weakly separated flows with separation length scales $\leq 2\delta$ whereas studies exhibiting a stronger downstream influence tended to have strongly separated flows with length scales $\geq 4\delta$.[15]

Although some of the earlier research points to the relevance of underlying hydrodynamic instabilities, the research findings are contradictory and therefore inconclusive. Thus, based on past and current research there is already a clear need for a fundamental and unequivocal understanding of the hydrodynamic instability mechanisms that are relevant for SBLI. The incomplete understanding of the underlying physical mechanisms for SBLI (in particular with regard to the low–frequency oscillations) poses a roadblock for the reliable and efficient operation of high–speed atmospheric flight vehicles. This lack of understanding is also the reason why effective and efficient active flow control (AFC) techniques are so difficult to realize for SBLI.

SBLIs in the presence of laminar approach flow are also of interest because of the insight that they may be able to provide into the more complicated transitional or fully turbulent cases. For a shock–induced laminar separation bubble, Robinet found a bifurcation of an initially 2D steady flow that, for increasing shock intensity, evolved into a 3D, stationary asymptotic state and eventually into a 3D unsteady state.[16] A secondary recirculation within the primary separation bubble characterized the three–dimensionality of the interaction region along with a spanwise velocity component. A global stability analysis was performed to explain the physical origin of the three–dimensionality and the presence of 3D unstable global mode was confirmed. Rist and co–workers examined the stability of hypersonic boundary layers over compression ramps and also in the presence of impinging shocks.[17,18] By comparing numerical simulations and experiments, they clearly showed that non–parallel effects led to increased growth rates of the disturbances.

Studies of laminar interactions, like turbulent, have devoted particular attention to the unsteadiness of the shock motion at relatively low frequencies with respect to the characteristic frequency of the boundary layer. The characteristics of the unsteadiness related to the separation shock and separation bubble have been widely reported in the literature and strong similarities are seen between various configurations commonly studied in SBLI, such as compression ramps, blunt fins, and impinging shocks. Reasonable agreement has been reported between numerical simulations and experiments, but as mentioned previously, the mechanisms that drive the unsteadiness remain unclear.

For practical applications, the consideration of 3D effects on SBLI is a must. Unfortunately, the 3D SBLI has received very little attention over the last decade. A somewhat limited body of research indicates that the unsteadiness observed in 2D SBLI carries over to swept cases. For a given shock strength, the RMS pressure and turbulence amplification decrease with increasing sweep and dominant separation shock frequencies increase. For example, on a 28deg compression ramp at M=5, the low-frequency unsteadiness shifted from 0.3-0.5 kHz (unswept case) to 2-7 kHz for 50deg sweep.[19] Qualitatively similar observations have been made for sharp fins.[20,21] However, a surprising gap exists in the literature for the fundamental case of a 3D pressure gradient imposed by a swept impinging oblique shock.

Three dimensional SBLIs can be classified according to whether the shock generator is dimensional or dimensionless and the latter can be further distinguished by whether the interaction has conical or cylindrical similarity.[22] Dimensional interactions include circular cylinders, blunt fins, swept forward facing steps, and other shock generators with an associated length scale. Dimensionless interactions include sharp fins, swept compression corners, swept oblique impinging shocks, and other shock generators with no associated length scale. Dimensionless swept interactions, which are most applicable to this work, have been reviewed extensively by Settles and Dolling.[23] The similarity of an interaction, conical or cylindrical, is determined by whether the size of the interaction changes over its span. For cylindrical similarity, this size is constant after an inception region. For conical similarity the separation and reattachment lines appear to radiate from a virtual origin (Figure 2). Similarity for sharp fins is almost exclusively conical.[21] Swept compression ramp interactions are found to exhibit cylindrical similarity for modest sweep angles and conical similarity once the sweep angle passes a given threshold.[22]

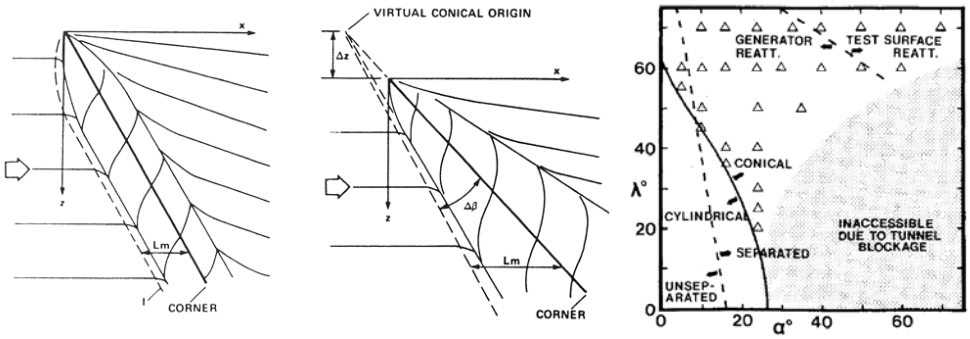

Figure 2: Left: Schematic of surface streak lines for cylindrical and conical similarity for swept SBLIs.[24] Right: Flow regimes for swept compression corner interactions (λ is sweep angle and α is corner angle) at Mach 2.95.[22]

Settles and Kimmel mapped out the conical and cylindrical similarity regimes for a swept compression corner at Mach 2.95 (Figure 2).[22] The boundary between the two regimes was found to be independent of both δ and Re*δ. These results were reproduced by Horstman using RANS calculations.[25] Settles and Dolling point out that the cylindrical/conical boundary moves to larger shock and sweep angles with increasing Mach number.[23] Holden investigated a swept oblique impinging shock SBLI at M=11 for very cold walls.[26] Wedge angles of 12.5 and 15 degrees and sweep angles of 0, 15, 30 and 45 degrees were considered. Cylindrical similarity was observed for all cases and some exhibited separation. The most surprising aspect of Holden's result was that the streamwise interaction length (defined as the distance from the impinging shock to the upstream extent of the plateau in heat transfer and pressure measurements) slightly decreased with sweep angle. This is in direct contrast to Settles experiments for an adiabatic swept corner at Mach 2.95. This inconsistency is examined in the experimental results reported here.

IV. Objectives and Approach

The objective of this work is to provide a fundamental physics-based understanding of the underlying instability mechanisms governing 3D SBLI through a combined approach of experiments, numerical simulations and stability analysis. In doing so, we will bridge the gap between 2D and 3D SBLIs. In particular, our intent is to focus of the effect of sweep on the interaction between impinging oblique shocks and turbulent boundary layers. In contrast to other swept interactions (e.g. corners and fins), impinging SBLIs constitute a more fundamental or canonical case because the boundary layer is not redirected by or reattached to the shock generator. Thus, the effect of a purely 3D pressure gradient can be studied. We will also explore laminar and transitional cases to provide additional insight into the physics.

In the following sections, our progress over the course of a one year award is summarized. Results from experiments, numerical simulations and stability analysis are provided. The experimental and numerical aspects of the work are noticeably separated in the text below. The experiment has taken the lead on defining parameters of interest while the simulations have focused primarily on code validation in year 1. Significant physical insight into SBLIs has been provided in both the experimental and computational cases. At present, the necessary tools for linking experiments and computations have been developed and a major focus of future efforts is to more closely link the research tracks.

V. Experimental Facilities and Techniques

A. Supersonic Wind Tunnel

A vacuum driven supersonic wind tunnel is used as the primary test bed. The tunnel has an adjustable throat allowing for Mach numbers between 1.5-5 in a clear test section. The 34 m^3 (1200 ft^3) vacuum tank is emptied by a 494 CFM Leybold SV360 pump. Full pump down time is ~10 minutes with recovery time

between runs of ~5 minutes. The optically accessible test section has dimensions of 8.5 × 3 × 4.75 in^3. The tunnel is equipped with an adjustable diffuser that allows run time of 15-30 sec depending on Mach. Shock generating wedges are positioned in the tunnel using a wall plug and sting arrangement. Stagnation conditions are atmospheric. The shock generators span 75% of the tunnel width, impose a 15° flow deflection (i.e. wedge angle), and are swept in the spanwise direction at 0, 22.5, 40°. A reversed 40° wedge was also tested, where the sweep runs in the opposite direction. This mirror image configuration is tested to check for any facility bias. The sweep angles are chosen based on Holden's test matrix to provide some preliminary answers to the streamwise interaction length discrepancy discussed above.[26] A mock-up of the wind tunnel with shock generator installed as well as close-up view of a swept wedge model is shown in Figure 3.

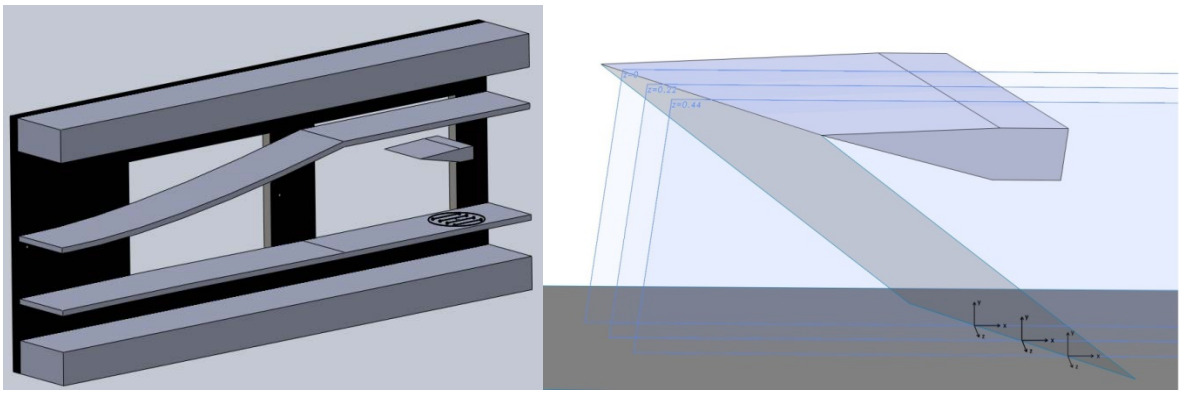

Figure 3: Notional schematics of wind tunnel experiments (not to scale).[27]

B. Particle Image Velocimetry

Stereoscopic PIV data are acquired using a LaVision (Davis 8) system consisting of two cameras (Imager CMOS 2560x2160 pixel 16 bit), PIV laser (Quantel Evergreen PIV 200 mJ, 15Hz) and necessary lenses, filters, mounts, timing unit and computer. The laser is used to illuminate submicron (~500nm) seed particles introduced into the entire laboratory to provide homogeneous seeding. A variety of GPU and CPU processing routines were compared until an acceptable set of GPU parameters was determined. Subsequently, GPU processing was used for all of the results presented herein as it decreased processing time substantially. For each image pair, subregions are preprocessed with a 16 pixel sliding background subtraction to reduce reflections then cross-correlated using decreasing window (32^2-16^2 $pixel^2$) multi-pass processing with a 50% overlap. The resulting velocity fields are minimally post-processed to remove vectors with peak ratio correlation coefficient below 0.1. Removed vectors are replaced by an interpolation procedure using neighboring vectors. A 3 x 3 Gaussian smoothing filter and polynomial filter are also applied to the calculated velocity field. An image mask was set on the wall so that the near surface and spatial resolution were approximately 0.24 mm (0.032 δ). For each test case, 900 samples were taken.

C. SBLI Coordinate System

The general characteristics of a SBLI induced by an impinging shock have been shown in schlieren imaging and a schematic in Figure 4. The interaction consists of an impinging shock, a reflected shock, a thickened boundary layer and sometimes separated region, a relaxation region, and an expansion fan. Both shocks are curved at the foot such that the bottom of the shock is nearly normal to the tunnel floor. The thickened or separated region (if present) begins shortly after the location where the reflected shock foot intersects the boundary layer and typically ends near the location at which the impinging shock intersects the boundary layer. The expansion fans are a result of the freestream tunnel area increasing when the boundary layer size decreases. The interaction length is defined as the distance between the x intercepts of linear extrapolations along the impinging and reflected shocks (see Figure 4b). This differs

slightly from the definitions employed, for example by Souverein et al. (2010) and Webb et al. (2013), wherein the curved shock foot of the reflected shock is used.[28,29] Our definition simplifies the extraction of the interaction lengths from PIV data, but increases the value by 15-25%. Regardless, the reported trends (if not the quantitative interaction length) should be consistent with other definitions.

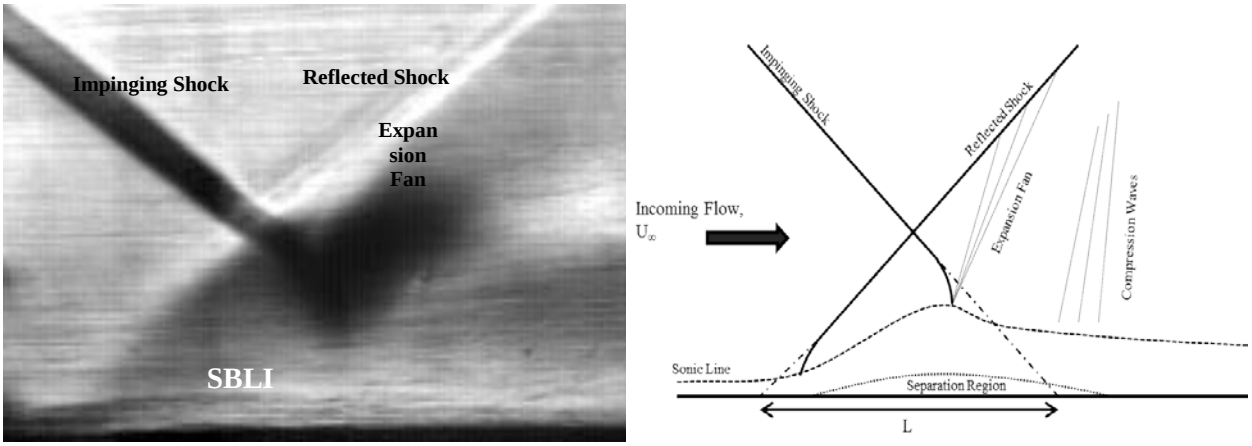

Figure 4: Impinging SBLI a) schlieren and b) schematic (not to scale).

PIV data was taken at three planes separated by 22% span (12.7 mm) and centered relative to the tunnel as shown in Figure 5. The planes are labelled such that z*=0, 0.22, 0.44 correspond to planes (subscripts) 0, 1 and 2 respectively, where z* is normalized by the span of the shock generator and equal to zero in the plane corresponding to the root of the interaction (the west plane for the initial experiment and the east plane for the mirrored experiment). The edge of the shock generator is at z* = -.28. The sweep line in Figure 5 denotes the location of the impinging inviscid shock wave as well as the location for the origin of the dimensionless coordinate system. This shift assists in better identifying the similarity and nature of the flow. More rigorously the streamwise coordinate $x_{0,1,2}$, (x_0 is the streamwise coordinate for plane 0), is shifted by $X_{0,1,2}$, the shock impingement location, and then nondimensionalized by the interaction length L in that plane, $x_{0,1,2}^* = (x_{0,1,2}-X_{0,1,2})/L_{0,1,2}$.This means that there are three separate coordinate systems corresponding to each measurement plane for each test piece resulting in a total of fifteen coordinate systems for the current analysis. For ease of interpretation, plots are presented showing the same dimensional space but with their local nondimensional coordinates employed as labels. It is also important to note that for simplicity the same δ is used for all cases. The boundary layer grows on the tunnel floor for approximately 750mm before reaching the SBLI with a maximum 25mm difference in growth length between different test cases due to sweep. Assuming incompressible turbulent boundary layer growth, we expect less than 2.7% change in boundary layer thickness, so it is reasonable to make this assumption.

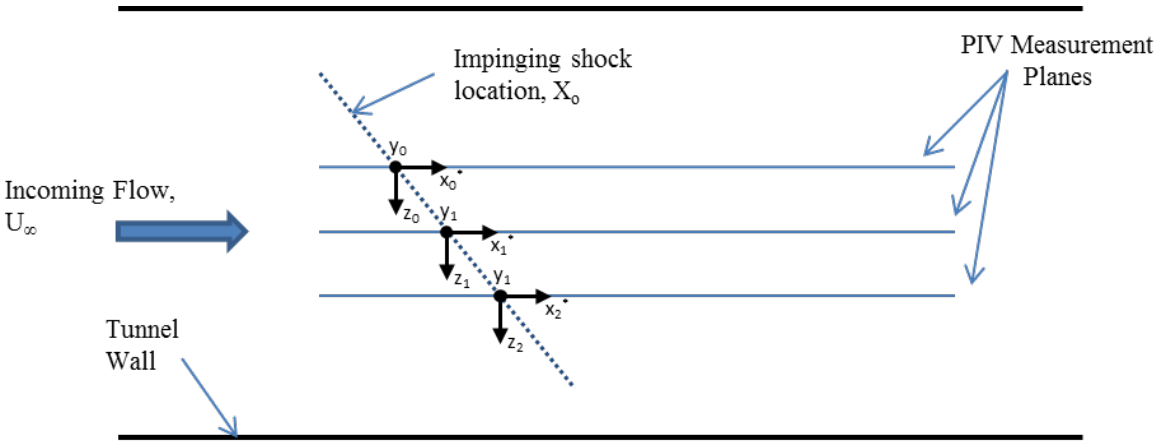

Figure 5: Measurement planes and coordinate systems (not to scale).[27]

VI. Experimental Results

A. Incoming Flow Characterization

The boundary layer profile for all three incoming planes is shown in Figure 6. This boundary layer profile was constructed using the velocity field from PIV. The data was taken at x_i^*=-1.2. This location is representative of the incoming boundary layer for both unswept and swept cases. The incoming boundary layers for all three planes collapse nicely onto a single profile, with all variations falling within the experimental uncertainty. Because of this homogeneity, a single average boundary layer thickness (7.6 mm) is used to normalize interaction length measurements. A Van Driest transformation and Maise-Macdonald model profile are shown in Figure 6b. The profile used a mixing length constant of 0.4 and a wake strength parameter of 0.5. The agreement of this profile with all three planes confirms that the incoming boundary layer is fully turbulent and fairly uniform across the span.

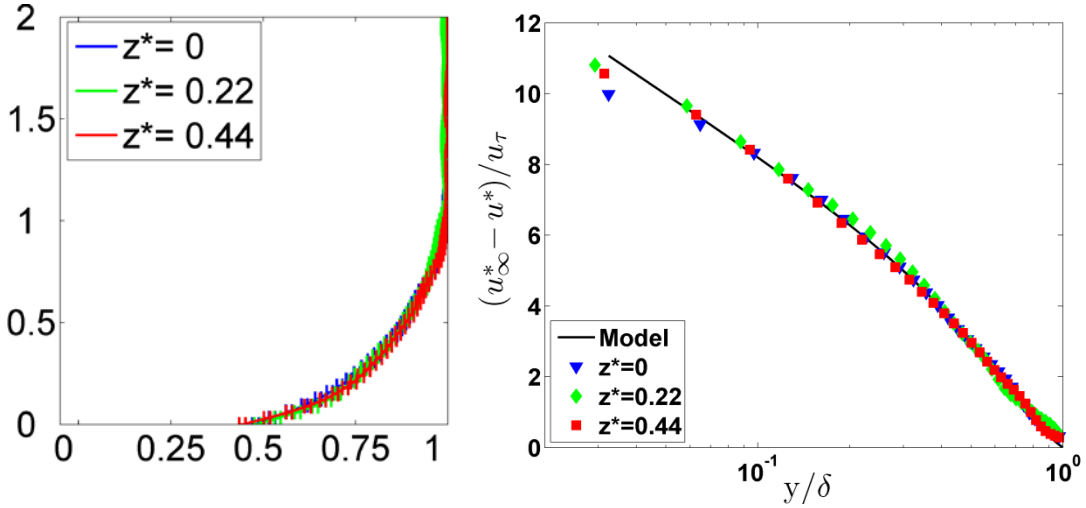

Figure 6: Incoming boundary layer a) profiles (y/δ vs. U/U_∞ b) Van Driest transformation and Maise-MacDonald model profile.[30]

Table 1 and Table 2 contain the incoming flow and boundary layer properties for all three planes in both experiments at x_i^*=-1.2. Several values have been calculated using both incompressible and compressible assumptions, with incompressible values listed first. The compressible values were calculated using the density approximation found in Maise and MacDonald.[30] These properties were mostly constant across the incoming boundary layer, with less than 10% variation across the different

spanwise planes. This variation is expected due to experimental uncertainty and spatial resolution of ±0.24mm. There are some differences between the two tables, most notably the Mach number, boundary layer thickness and Reynolds number. These changes were caused by a combination of experimental uncertainty and modifications to the tunnel made between experiments. The pressure taps, gaskets on the removable tunnel wall, and adjustable throat were all repaired, which eliminated an unsteady behavior previously observed at the west wall of the tunnel (near Plane 0). Because of the differing experimental conditions, the unswept wedge experiments were repeated along with the mirrored 40 degree wedge, in order to confirm the mean flow behavior and particularly the similarity (cylindrical vs. conical). In both cases, the incompressible shape factor of 1.3-1.4 classifies this boundary layer as fully turbulent, which is to be expected for the associated Reynolds number.

Table 1: Incoming boundary layer characterization for initial experiment

Plane	M_∞	U_∞ (m/s)	P_o (kPa)	T_o (K)	δ (mm)	δ* (mm)	θ (mm)	H	Re_θ
Z* = 0	2.3	550	698	298	7.8	2.4, 1.2	0.60, 0.88	4.0, 1.4	5.9,8.6 x 10^3
Z* = 0.22	2.3	540	698	298	8.4	2.5, 1.3	0.67, 0.93	3.8, 1.4	6.4,8.9 x 10^3
Z* = 0.44	2.3	550	698	298	7.7	2.7, 1.3	0.70, 0.96	3.8, 1.4	6.9,9.4 x 10^3

Table 2: Incoming boundary layer characterization for mirror wedge experiment

Plane	M_∞	U_∞ (m/s)	P_o (kPa)	T_o (K)	δ (mm)	δ* (mm)	θ (mm)	H	Re_θ
Z* = 0	2.4	560	701	298	7.9	2.5, 1.2	0.61, 0.87	4.1, 1.4	5.8,8.2 x 10^3
Z* = 0.22	2.4	560	701	298	7.0	2.1, 0.95	0.55, 0.76	3.8, 1.3	5.3,7.3 x 10^3
Z* = 0.44	2.4	560	701	298	7.1	2.2, 1.1	0.56, 0.79	4.0, 1.4	5.4,7.7 x 10^3

D. Mean Velocity Fields

Wall normal velocity contours are shown in Figure 7 and Figure 8. Note that while each plot has axis labels based on the interaction length for that plot, the spatial domain shown is the same, allowing for direct visual comparison. Figure 7 shows the initial test matrix, with the unswept, 22.5 degree swept, and 40 degree swept wedge. Streamlines have been drawn on the plots, with additional streamline rakes added at x* = -0.75, -0.5, and -0.25. It is clear from the streamlines that reversed flow occurs in almost every case near x* = -0.25, with the possible exception of the 40 degree swept wedge in the Plane 0. The red and yellow triangular region in each plot is a visual confirmation that the 40 degree swept wedge has conical similarity, while the 22.5 degree and unswept wedge have cylindrical similarity. The region of high V_y is bounded by the reflected and impinging shock, so its size should correlate directly with the interaction length. It is clear in these figures that the interaction length for the 40 degree swept wedge increases from plane 0 to plane 2 (in the direction of sweep), while the other two wedges have relatively constant interaction length in each plane. Another trend, also suggesting conical similarity, can be seen in the negative V_y region downstream of the impinging shock. For the 40 degree swept wedge, the magnitude of this region increases drastically moving from plane 0 to plane 2. There is a slight increase in this magnitude for the 22.5 degree swept wedge, and it stays relatively constant between planes for the unswept case.

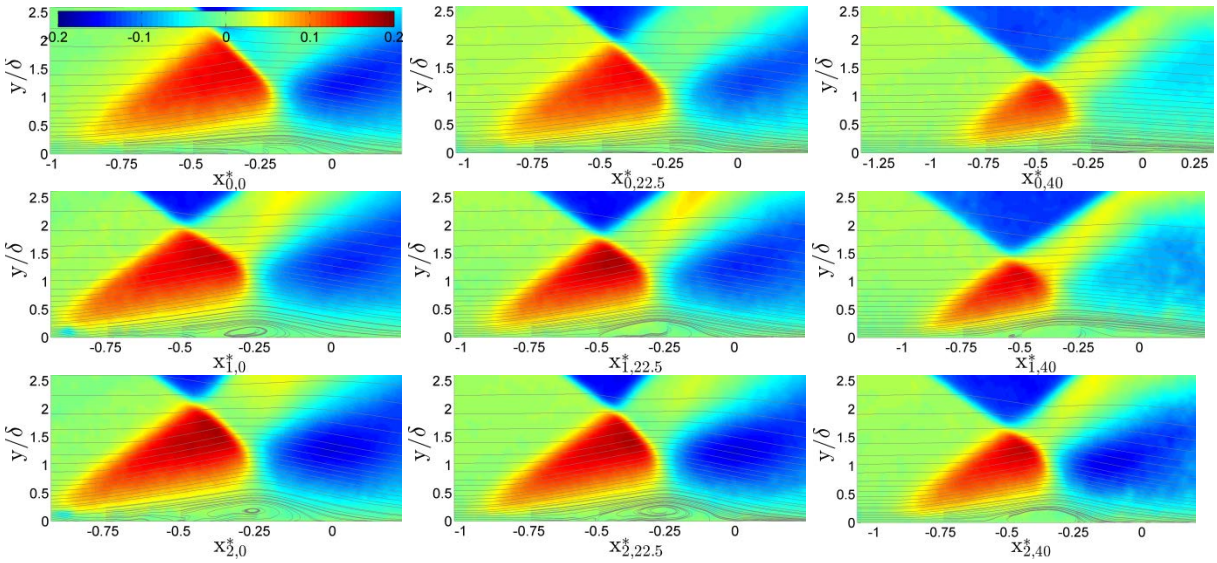

Figure 7: Contours of mean wall normal velocity with streamlines for the initial experiment.[31] Unswept, 22.5 degree sweep and 40 degree sweep are shown from left to right while the direction of sweep is down the page.

The V_y contour plots for the mirror wedge are shown in Figure 8. Both trends seen in the interaction region of Figure 7 are reproduced here, which confirms that they are due to the interaction itself and not from any nonuniformity of the tunnel. The red triangular region representative of the interaction increases in size between plane 0 and plane 2 for the 40 degree swept wedge and stays constant for the unswept wedge. The negative V_y region after the impinging shock increases in magnitude between planes 0 and 2 for the 40 degree swept case and stays constant for the unswept case. The mean velocity for this case does not show reversed flow for the 40 degree swept wedge. However, individual frames show reversed flow on the order of 5m/s (1% U_∞). This is in contrast to the initial experiment in which the 40 degree swept wedge showed a small amount of reversed flow in the mean for 2 out of 3 planes. This discrepancy is possibly due to the increased Mach number coupled with the fact that the reversed flow in the initial data set was not clearly outside the measurement uncertainty.

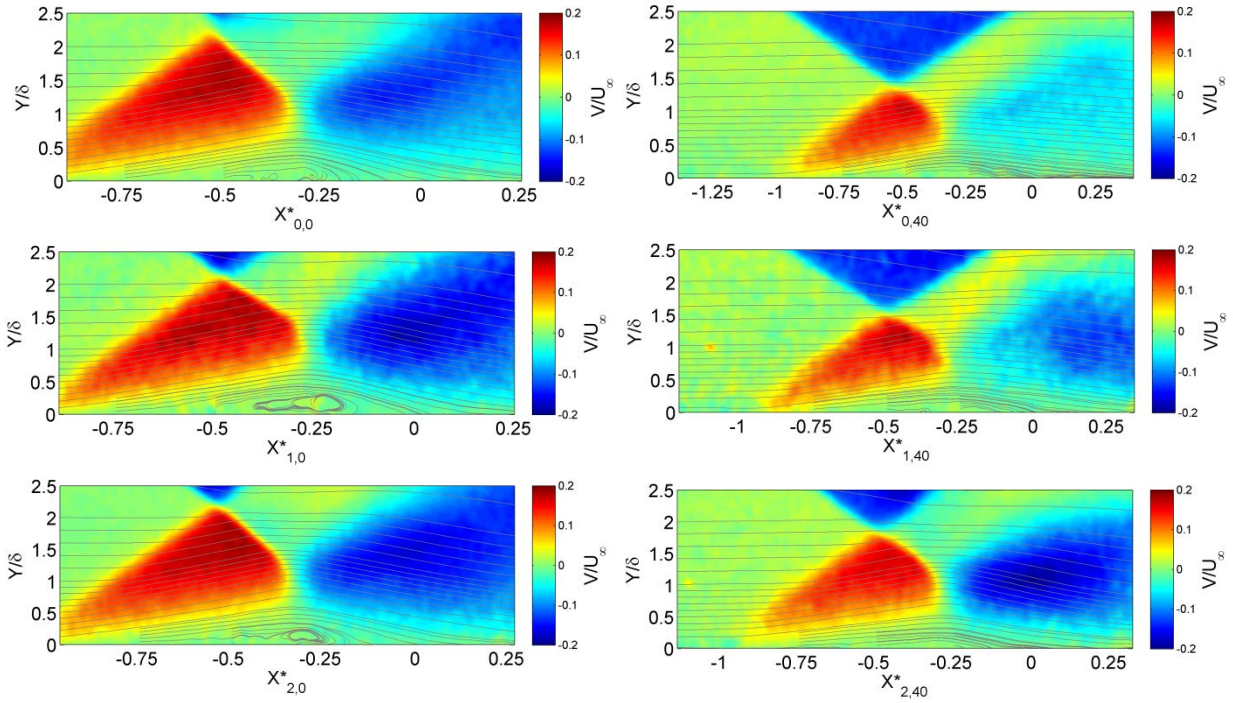

Figure 8: Contours of mean wall normal velocity with streamlines for the mirrored experiment.[27] Unswept and 40 degree sweep are shown at left and right while the direction of sweep is down the page.

E. Interaction Length Trends

Interaction lengths are shown in Figure 9. These values were found using a custom-made Matlab script similar to that used by Klomparens et. al. (2015) for unsteady shocks.[32] This script was applied to both data sets, initial and mirrored. This script relies on an initial user guess of the shock location and angle, though analysis showed that errors in the user input do not create errors in the calculated shock position or angle. The operation of the program proceeds according to the following steps. First, the vector field is subdivided into two sections, one for the impinging shock and one for the reflected shock. The *V* vector field for each section is transformed into an intensity image, with the intensity representing the magnitude of the *V* velocity. A Wiener adaptive 2D lowpass filter is applied to smooth out noise. The image is then processed with a morphological closing routine which smooths out all sections parallel to the initial guess using lines as the morphological operators. Subsequently, a Canny filter and a Sobel filter are applied to the image and then combined to create a full set of the lines in the image. Finally, a Hough transform is applied to find straight lines within the Canny/Sobel filtered set of lines. This Hough transform is limited to lines angled ± 10 degrees from the initial input in order to avoid finding extraneous lines that do not correspond to the shock. This process is verified by the user to ensure that the program correctly identifies the shock position and angle. With proper filter settings, this program formed a robust method for finding shock waves even in highly turbulent or noisy vector fields. Once the shock position and angle have been found, the Matlab script is used to find the interaction lengths by extrapolating the shock lines down to the floor position. The interaction length data is filtered in two steps, the first of which being to eliminate the results from found shock lines that are significantly shorter than the rest of the shock lines (roughly 1/6 of the shocks). Because of the uncertainty in the filtering and Hough transform, these short lines are either flow features other than shock waves or are much more likely to generate error when extrapolated. The longer set of found shock lines cover a wider amount of vector data and tend to be more precise. The data is then filtered to eliminate any shocks and associated interaction lengths where the shock angle, shock position, or interaction length fell more than three standard deviations from the respective mean.

The interaction lengths were normalized against the incoming boundary layer thickness. The spanwise trends in L/δ are shown in Figure 9. As previously stated, two unswept cases are provided for reference, corresponding to the two different sets of incoming flow characteristics from the initial and the mirrored experiment. Figure 9a shows the results from an analysis of the mean data, while Figure 9b shows the results from an analysis of the instantaneous vector fields. Comparing the two shows that while both methods resulted in slightly different interaction lengths, the general trends are the same. Moreover, the trends in the data remain the same between the initial and mirrored sets of data. The forty degree case shows a linear increase in interaction length across the three planes, while the other two cases have constant interaction length in all three planes, within uncertainty. The fact that these trends are recovered for the mirror wedge, despite moderate changes to the tunnel between the experiments, verifies that the results of the previous study were not tunnel dependent. This furthers the conclusion that the transition to a conical shock / boundary-layer interaction occurs before a 40 degree sweep angle for these flow conditions. Conical similarity is perhaps just beginning to occur in the 22.5 degree case. The unswept case deviates slightly between the initial experiment and mirrored experiment. Because of the significant modifications to the wind tunnel and the different incoming flow properties, this was not entirely unexpected.

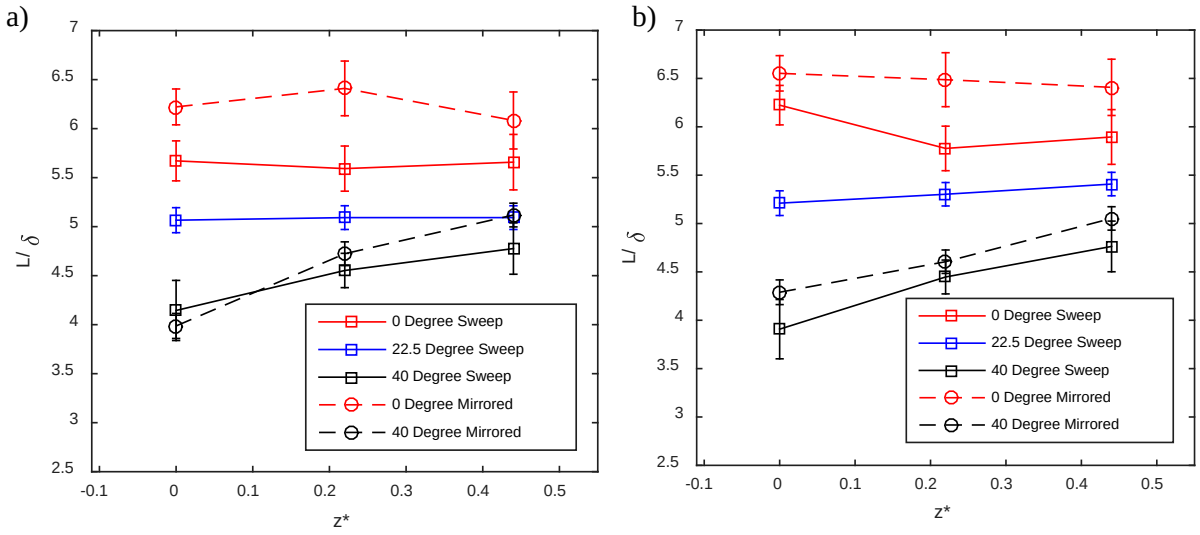

Figure 9: Normalized interaction lengths vs. Spanwise location, taken from a) mean flow data and b) instantaneous data.[27]

F. Summary of Experimental Results

The interaction between a swept impinging oblique shock and a turbulent boundary layer has been studied with stereoscopic PIV at Mach numbers of 2.3. The impinging shock is created by a 15º wedge that is swept back at 0º, 22.5º and 40º, along with a mirrored 40º wedge (swept the opposite direction relative to the wind tunnel). The 0 and 22.5 degree cases are strongly separated with L/δ > 5 in all spanwise planes. The 40 degree case displays a weaker interaction with L/δ between 4 and 5. The interaction length decreases with increasing sweep angle across the test matrix. The unswept and 22.5 degree swept cases are both found to have cylindrical similarity while the 40 degree swept interaction demonstrates conical similarity. The mirrored data set confirms these trends of conical and cylindrical similarity despite moderate modifications to the wind tunnel. All cases, except plane 0 for the 40 degree wedge (i.e. root), show separated flow in the interaction region and some contain reverse flow that is clearly outside of the measurement uncertainty. A comparison with the very limited amount of literature on this type SBLI shows varying levels of agreement. Interaction length decreases with sweep consistent

with similar studies by Holden in hypersonic conditions, but is inconsistent with swept compression corner data in supersonic flows which shows an increase in L/δ. Conversely, the nature of the highly swept interaction (conical) is in agreement with swept compression corners in supersonic flow, but disagrees with the interaction observed in hypersonic flow (cylindrical). Inconsistencies in the Mach number (supersonic vs. hypersonic) and method of shock generation (impinging vs. corner) likely explain the agreement/discrepancy in these results.[22,26]

VII. Computational Effort

The initial focus of the computational portion of this study was on adapting and validating an in-house developed DNS research code for use in SBLI. The interaction of an oblique shock wave and a laminar boundary layer was chosen for this task. The flow parameters are taken from a benchmark SBLI data set in which the approach boundary layer is laminar Hakkinen et al. (1959).[33] The Mach number is 2.0 and the Reynolds number is 2.96×10^5, based on the impingement location for an inviscid case. A shock generator plate is emulated to create an oblique shock that impinges on the boundary layer causing separation. This is similar to the experimental aspect of this work, but in this case a laminar approach boundary is chosen to first validate the DNS. A number of different shock inclination angles were studied by Hakkinen et al. (1959), but our initial focus is on a 2D configuration with a wedge angle of $\theta = 3$ degrees, corresponding to a shock angle $\sigma = 32.58$ degrees and an overall pressure ratio between pressure after the reflected shock and the upstream pressure of 1.4. The variation of viscosity with temperature is assumed to obey Sutherland's law, for which the value of the Sutherland constant temperature is $T^* = 110.4$K and the freestream temperature is $T^*_\infty = 288.0$K. The main simulation parameters used for the results presented in this report are provided in Table 3.

Table 3: Flow parameters used in the simulations based on the conditions in the experiments conducted by Hakkinen et al. (1959).[33]

Flow Parameters :		
Re	$[-]$	$2.96 \cdot 10^5$
M	$[-]$	2.00
T^*_∞	$[K]$	288.00
Pr	$[-]$	0.72
γ	$[-]$	1.40
θ	$[degree]$	3.00
σ	$[degree]$	32.58

VIII. Governing Equations and Numerical Methods

A. Governing Equations and Numerical Scheme

The physical problem under consideration is governed by the compressible Navier–Stokes equations, consisting of conservation of mass, momentum and total energy. The fluid is assumed to be an ideal gas with constant specific heat coefficients. The Navier–Stokes equations are integrated in time with a standard 4th-order accurate Runge–Kutta scheme. The spatial discretization is based on high-order

accurate finite differences. In particular, the derivatives of the viscous terms and the source term are calculated by 6th-order non-compact central finite differences in the streamwise direction and by 4th-order central finite differences in the wall-normal direction. The inviscid fluxes are divided into an upwind flux and a downwind flux using van Leer's splitting.[34] Then, grid centered upwind differences with 9th-order accuracy are applied to evaluate the derivatives for these fluxes.[35] This high–order accurate finite difference code was developed in our CFD Laboratory for supersonic/hypersonic transition research for flat–plate and conical geometries. For a detailed description of the DNS code see Laible et al.[36,37]

G. Boundary Conditions

The inflow boundary for supersonic boundary layer simulations is split into two regions: a subsonic region close to the wall and a supersonic region away from the wall. In the supersonic region, Dirichlet conditions for u, v, w, T, p and ρ are specified (obtained from the similarity solution). For the subsonic region in the boundary layer, the non-reflecting boundary condition suggested by Poinsot and Lele is adopted.[38] On the flat–plate surface, the no-penetration (v = 0) and the no-slip (u = 0, w = 0) conditions are enforced. The wall is set to be isothermal with the temperature equal to the laminar adiabatic wall temperature. The value of the pressure at the wall boundary is obtained from the y-momentum equation. Finally, density is computed using the equation of state. At the outflow, the second derivatives of the primitive variables are set to zero. Density is again determined from temperature and pressure by using the equation of state.

The boundary conditions at the freestream boundary are applied in a different manner for the computations of the flow without SBLI and with SBLI. To calculate the steady flat–plate solution with no shock, a characteristic boundary condition according to Harris is used.[39] For the SBLI simulations, the steady solution with no shock is specified within the whole integration domain as initial condition. At the start of the SBLI simulation, the shock condition is introduced at the freestream boundary. For several grid points upstream and downstream of the shock location the relevant flow variables are held constant. Elsewhere, the characteristic boundary condition is used. The variables downstream of the shock location at the freestream boundary are calculated by the Rankine–Hugoniot relations. A steady shock then establishes itself within the entire flow field during the calculation.

IX. Computational Results

Skin friction and wall pressure at the plate are presented in Figure 10 and are compared with results from Hakkinen et al.,[33] Katzer[40] and Sandham et al.[41,42] As expected, the results show rapid changes near the separation and reattachment and a pressure plateau in the bubble region. The pressure ratio reaches a value of 1.4 downstream of the reflected shock in accordance with the Rankine-Hugoniot relations. Both upstream and downstream of the separated flow region, the skin friction curve follows the laminar solution.

The calculation results are quite similar to the experimental measurements. However, the calculated skin friction and wall pressure differ from the benchmark data. The calculated separation bubble is slightly longer in the present study. Possibly, the three–dimensional effects present in Hakkinen's experiment, and/or the effects of freestream turbulence may reduce the bubble length when compared to our two–dimensional numerical calculations and those published in the literature.[40,42] Katzer also obtained a longer bubble than in the experiments, however it is shorter than ours and those from other recent two–dimensional numerical calculations. The reasons for these differences have been investigated by Sansica et al. [41] They also studied the effect of using different models for calculating the viscosity as a function of temperature on the bubble length. They concluded that the different methods used to calculate the viscosity do not affect the bubble length. Note that for the simulations presented, Sutherland's law with $T^* = 110.4K$ is used. Our present results closely match those by Sandham and co-workers.[41]

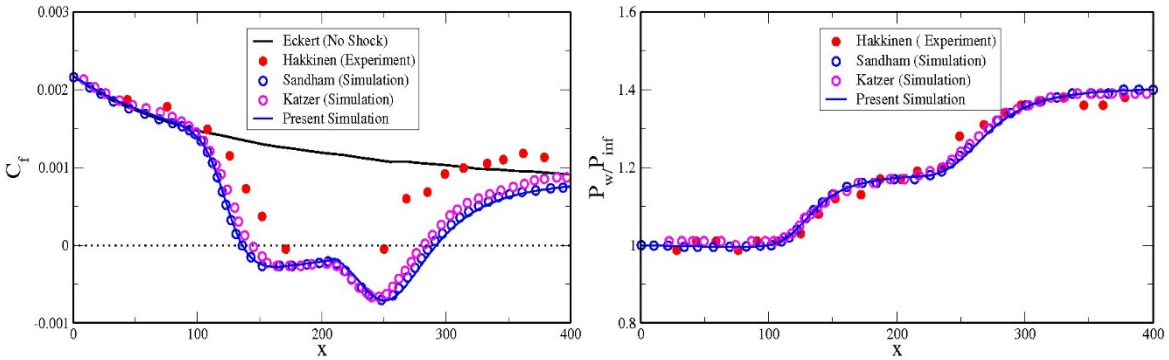

Figure 10: Streamwise distribution of skin friction and wall pressure. M = 2.0, T^*_∞= 288.0K, θ = 3 degrees, Re = 296,000.[43]

Contours of density and wall–normal velocity, both with streamlines, are shown in Figure 11. As the shock wave impinges on the laminar boundary layer, it causes separation of the flow. Both the impinging and reflected shock are clearly visible. In addition, the separation bubble shows asymmetric behavior, which is in agreement with asymmetric skin friction distribution in Figure 10. A lower minimum is observed at the back of the bubble due to the center of recirculation being shifted downstream. The wall-normal velocity shows qualitatively similar features as the turbulent SBLI results from the experiment. The domain size is chosen such that the reflected waves of the impinging shock leave the domain at the outflow boundary.

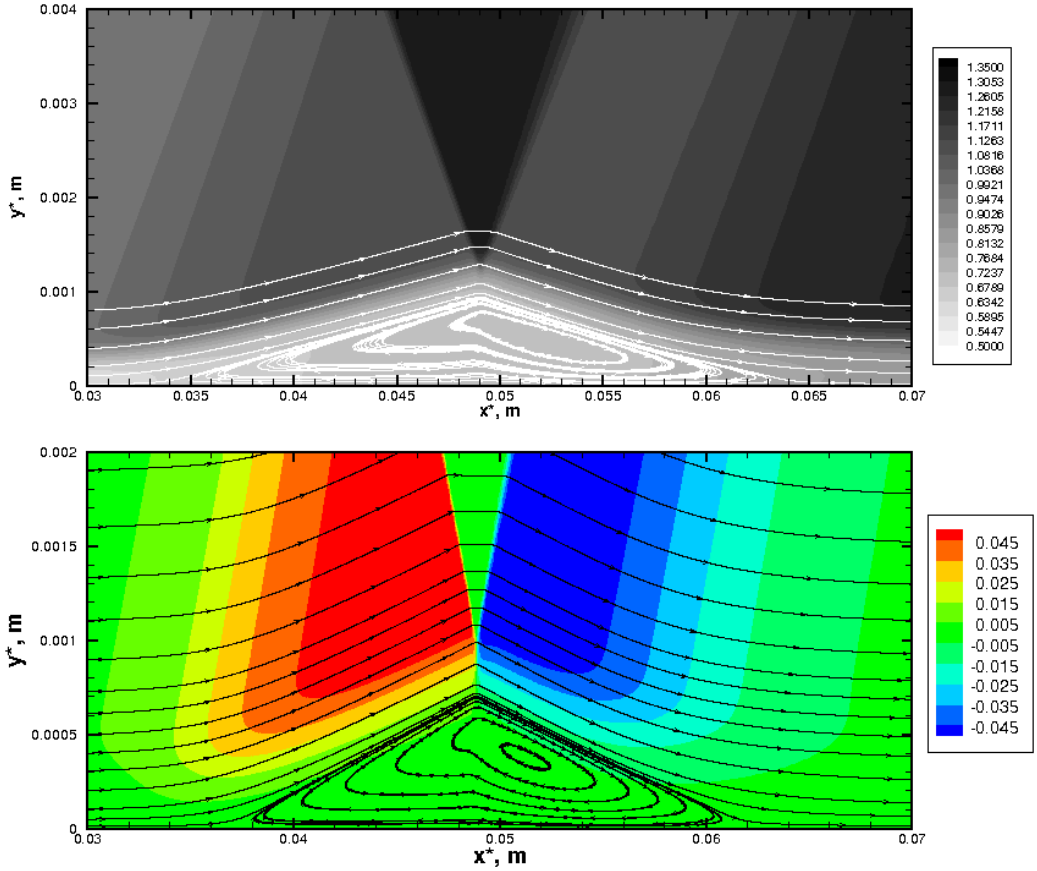

Figure 11: Contours of (top) density with streamlines and (bottom) wall–normal velocity with streamlines. M = 2.0, T^*_∞= 288.0K, θ = 3 degrees, Re = 296,000.[43]

A. Linear Stability Investigations

The development of low–amplitude disturbances has been investigated in order to establish the stability of the flow in the presence of a laminar separation bubble generated by the SBLI. Two- and three–dimensional pulse disturbances with a broad spectrum in frequency[44] are introduced into the boundary layer for cases with and without SBLI. The pulse disturbance develops into a wave packet that propagates downstream which has a broad spectrum in frequency and wavenumber. This allows investigation of the response of the shock–induced separation bubble to both low– and high–frequency disturbances. For these computations, a linearized compressible Navier-Stokes solver is employed.[45] Detailed information on the flow stability is provided in Sivasubramanian and Fasel[43] and only a sample of results is provided here in the interest of brevity.

The wave packets spread in downstream direction and their amplitude levels increase as they propagate. In both 2D and 3D cases, the waves are much more strongly amplified by the presence of the SBLI. According to linear stability theory for supersonic boundary layers, the dominant disturbances (most strongly amplified) are three–dimensional (oblique disturbance waves). Therefore, the development of three–dimensional disturbances using a pulse for spanwise wave number 0.9/mm (the most amplified spanwise wave number at the impingement location) is investigated.

The amplitude of the waves within the wave packet are extracted and compared in Figure 12. This includes both two–dimensional and three–dimensional disturbances with and without SBLI. It is clear that both two–dimensional and three–dimensional (oblique) disturbances are more strongly amplified with the SBLI. In the presence of SBLI, the amplification of the 3D disturbance is particularly noteworthy in that it exceeds all others by nearly two orders of magnitude (Figure 12d).

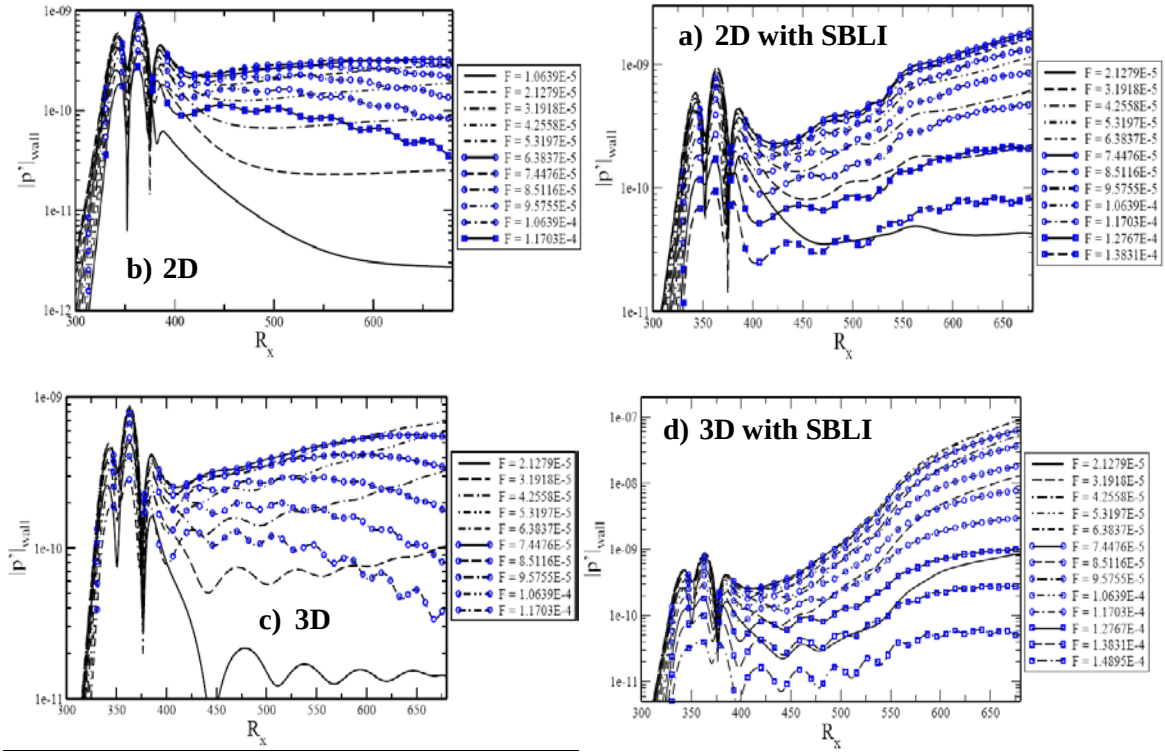

Figure 12: Streamwise development of the wall pressure disturbance amplitude for 2D and 3D (spanwise wavenumber, β=0.9/mm) disturbances with and without SBLI. M = 2.0, T^*_∞= 288.0K, θ = 3 degrees, Re = 296,000.[43]

H. Effect of Shock Angle and Reynolds Number

The effect of the incident shock angle was investigated by increasing the angle of the shock generator angle (θ) to 6 degrees while maintain Re=296,000. This produced a stronger pressure jump and consequently a larger separated flow region (Figure 13a). The separated flow region is now unsteady and sheds vortices. Increasing the Reynolds number to 500,000 (based on the impingement location for an inviscid case) while retaining θ= 6 degrees results in even stronger vortex shedding (Figure 13b). The increased Re reduces the boundary layer thickness. Therefore, the length of the separation bubble is also reduced. The stronger shedding may also play a role in the reduction in length.

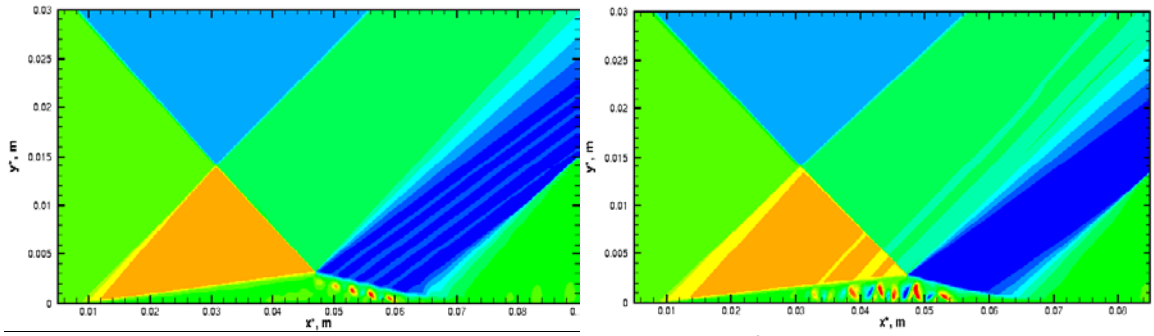

Figure 13: Contours of wall normal velocity for (left) M = 2.0, T^*_∞= 288.0K, θ = 6 degrees Re = 296,000 (left) and (right) M = 2.0, T^*_∞= 288.0K, θ = 6 degrees, Re = 500,000.[43]

The frequency spectra of wall pressure are presented in Figure 14. The spectra show distinct peaks at higher frequencies that correspond to vortex shedding for both Reynolds numbers. The high frequency peaks are due to a Kelvin-Helmholtz type instability mechanism arising from the inflectional velocity profile in the shear layer that forms between the flow inside the separation bubble and the flow outside the bubble. These are primarily observed in the aft part of the bubble. Peaks in the spectra are also observed for lower frequencies which may be associated with "breathing" of the bubble and the well-known low-frequency unsteadiness in SBLIs. "Breathing" refers to the dynamics of the bubble that includes a slow enlargement and shrinking of the bubble. The high Re case shows a much clearer low frequency "breathing" activity that is located farther upstream (x*≈0.045).

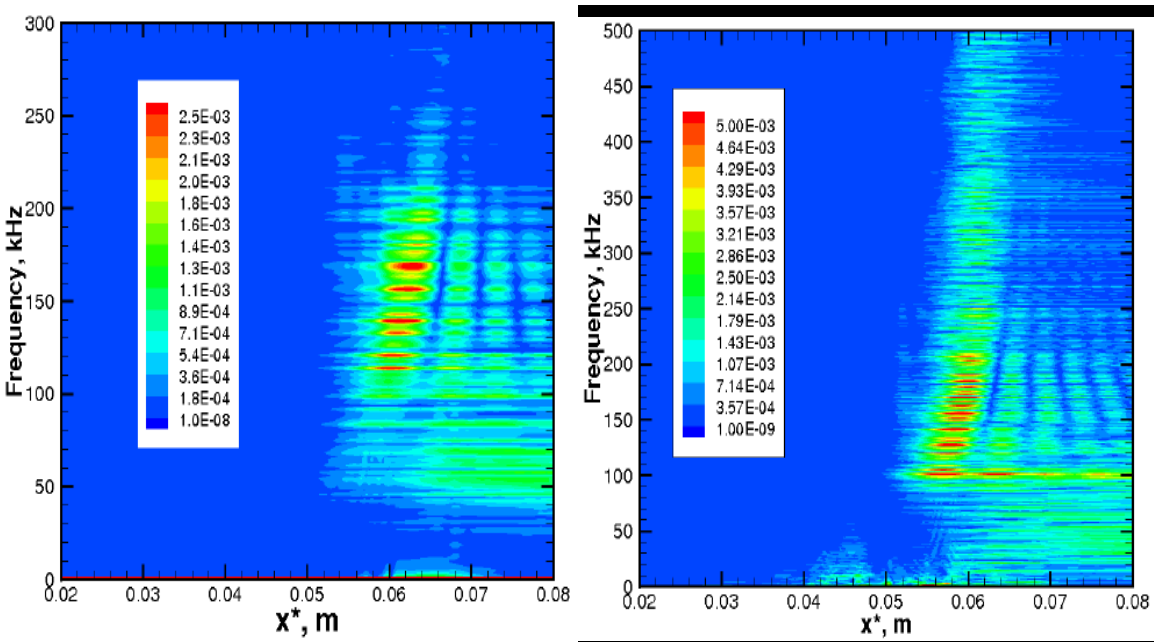

Figure 14: Frequency spectra obtained from wall pressure for (left) M = 2.0, T^*_∞= 288.0K, θ = 6 degrees Re=296,000 and (right) M=2.0, T^*_∞=288.0K, θ=6 degrees, Re= 500,000.[43]

Three–dimensional simulations for the high Reynolds number case have been performed to investigate the laminar–turbulent transition process in the presence of SBLI. Results from the three-dimensional direct numerical simulation are presented in Figure 15. Contours of instantaneous wall normal velocity are shown in the $x-y$ plane for a fixed spanwise location (z^* = 0.0). The vortex shedding that results from the shear layer instability (Kelvin-Helmholtz) is clearly visible and downstream of the reattachment location the flow seems to transition to turbulence. A close observation of the dominant flow structures and their streamwise development can provide further insight into the transition process. In Figure 15b the flow structures from the three–dimensional simulation are plotted using the Q criterion. The flow structures reveal the typical evolution due to a Kelvin-Helmholtz instability mechanism. During the early stages of the transition process, the dominant flow structures are the spanwise coherent vortices (or rollers) that arise from the vortex shedding (due to Kelvin-Helmholtz instability). Further downstream, the spanwise coherent structures become modulated in the spanwise direction, which may be due to the interaction o with three–dimensional disturbances. The spanwise modulation of these rollers increases as they propagate downstream and they eventually breakdown into small scale structures as the flow transitions to turbulence.

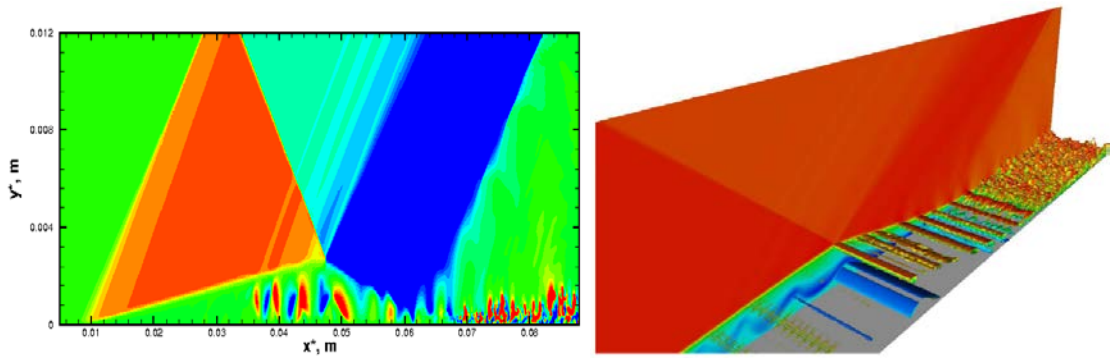

Figure 15: Contours of wall normal velocity for in a single x-y plane (left) and Q-criterion (Q=65000) (right). M = 2.0, T^*_∞= 288.0K, θ = 6 degrees, Re = 500,000.[43]

Figure 16 displays contours of streamwise velocity in the $x-z$ plane (parallel to the wall). This figure illustrates various flow features in the early turbulent region. Dark regions denote low-velocity flow and brighter regions correspond to high velocity flow. Remarkable streamwise structures seem to appear before the flow breaks down into small–scale structures. These streamwise structures may be a consequence of a dominant physical mechanism playing a role in the natural transition process in SBLIs. These mechanisms will be investigated in detail in future research. Note that such streamwise structures have also been observed in the numerical simulations of transitional SBLIs in hypersonic flows by Sandham et al.[46]

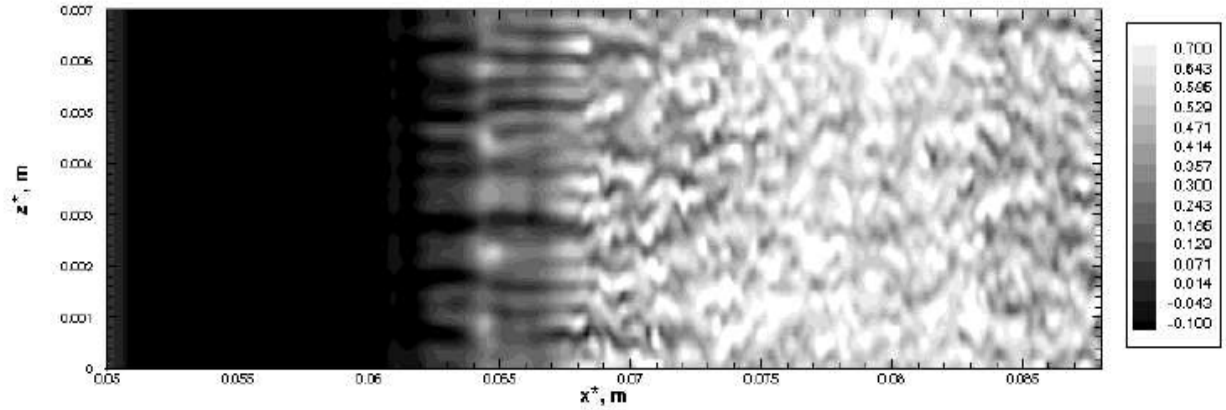

Figure 16: Contours of the instantaneous streamwise velocity in the x-z plane from 3D simulation. M = 2.0, T^*_∞= 288.0K, θ = 6 degrees, Re = 500,000.[43]

I. Summary of Computational Results

Direct numerical simulations (DNS) of laminar SBLI for a supersonic boundary layer at Mach 2 were performed at conditions matching classical benchmark experiments. The skin friction and pressure variation in the downstream direction from the simulation favorably compared to the experimental measurements and other numerical results published in the literature. The development of low–amplitude disturbances generated by a short duration pulse disturbance was investigated in order to shed light on the linear stability behavior of the flow in the presence of SBLI. It was found that both the two–dimensional and three–dimensional disturbances were more strongly amplified for the cases with SBLI present due to the increased instability effects of the adverse pressure gradient and boundary layer separation caused by the impinging shock wave. The 3D disturbances in the presence of SBLI are particularly noteworthy in that amplification exceeded all other cases by approximately two orders of magnitude.

Larger shock angles produce a stronger pressure jump and thus a larger and stronger separated flow region. As a consequence, the flow became unsteady and the bubble started to shed vortices likely due to a Kelvin-Helmholtz instability. The time history and frequency spectra of the wall pressure indicated the presence of both high- and low–frequency disturbances. The higher frequencies corresponded to the vortex shedding, while the lower frequencies are believed to be associated with the "breathing" of the bubble. Increasing the Reynolds number decreased the thickness of the boundary layer and the streamwise extent of the separated flow region was reduced. The time history of the wall pressure for the higher Reynolds number case clearly showed the low frequency "breathing" of the bubble which appeared as a distinct peak at a very low frequency in the frequency spectra consistent with low frequency oscillations in the literature.

Three–dimensional direct numerical simulations were performed for the higher Reynolds number case to investigate the laminar–turbulent transition process in the presence of SBLI. Flow visualization revealed a Kelvin-Helmholtz instability mechanism that lead to the development of spanwise rollers in the early stage of transition. Further downstream, the contours of the streamwise velocity component revealed streamwise structures ("streaks") before the flow breaks down to small scales as it transitions to

turbulence. These streamwise structures could be due to a secondary instability mechanism that may be relevant in a "natural" transition process.

X. Conclusions

Significant research findings have already been established over the course of our one year award. From the experimental side, both cylindrical and conical similarity have been identified for swept shocks impinging on a turbulent boundary layer. For the conditions surveyed (see Tables 1 and 2), cylindrical similarity is observed for the 0^o and 22.5^o cases while conical similarity is present at 40^o. The boundary between cylindrical and conical flow appears to be very near the 22.5^o swept case. The existence of both similarity types agrees with trends seen in compression ramps. The interaction length decreases with sweep angle for both similarity types. This decrease is more prominent for conical similarity. The decrease in interaction length agrees with studies by Holden for impinging shocks in hypersonic flows even though only cylindrical interactions were observed in the cited work, presumably due to weaker incident shocks.[26] However, this decrease is in contrast with Settles work and others on compression ramps. This disagreement has been identified previously in the literature[23] and is confirmed here in the presence of both cylindrical and conical flows. All of the surveyed interactions show a high probability of separation in the mean flow and instantaneous velocity fields show reverse flow that is outside of the measurement uncertainty. In addition, velocity profiles in the separated region show 3D effects which generally increase with sweep. The experimental results outlined here provide some context to the contrasting observations of swept impinging SBLIs in supersonic and hypersonic flows. It is now apparent that both cylindrical and conical interactions are possible, but the streamwise interaction lengths in the impinging case generally decrease with increasing sweep.

On the numerical side, an in-house developed high-fidelity, compressible Navier-Stokes solver has been modified for fundamental research of SBLI High-order accurate shock capturing schemes and boundary conditions have been implemented to generate impinging shocks. The resulting code has been validated using a well-known laminar SBLI experiment as well as other numerical studies for comparison. The influence of shock strength and Reynolds number on initially laminar interactions shows the development of both a Kelvin-Helmholtz and a bubble "breathing" type instability resulting in low- and high-frequency pressure spectra, respectively. This low and high frequency behavior is in qualitative agreement to widespread results in the SBLI literature. Implemented methodologies to generate a turbulent boundary layer at the inflow are currently being tested and validated.

XI. Future Work

The overarching focus of future work is to more closely link the experiments and simulations. From the experimental side, the study will examine turbulence characteristics, surface flow visualization and proper orthogonal decomposition to provide additional insight into the turbulent SBLI. In addition, plans for an upgraded wind tunnel test section complete with additional instrumentation (e.g. high bandwidth pressure sensors) are underway. A highlight of the future experimental research is tomographic PIV which is particularly relevant for clarifying the 3D nature of the interaction. This measurement would remove uncertainties with repositioning of the experimental hardware and allow interpretation of flow physics based on instantaneous measurements of the relevant fluid volume.[5] The experiment will also be expanded to include lower Re studies that are tractable for DNS.

On the numerical side, we plan to explore in detail the dominant physical mechanisms that play a role in the natural transition process in the presence of SBLI for supersonic boundary layers. We will also investigate SBLI when the approach boundary layer is completely turbulent in the presence of a swept shock. The flow parameters for these future investigations will be such that the conditions in the experiments will be matched as close as possible. Stability theory will be used in an attempt to provide a unifying link between experiments and simulations throughout the project.

XII. Publications

To date, the research project supported 3 conference papers and 1 M.S. thesis. Additional conference papers and journal articles are in preparation. A list of the current publications is provided below.

Conference Papers

1. Hainsworth J., Dawson, R. and Little, J., "Experimental Study of Unswept and Swept Oblique Shock-Turbulent Boundary Layer Interactions," AIAA Paper 2014-2738.
2. Dawson-Ruiz, R., Pederson, C. and Little, J., "Effects of Sweep on Impinging Oblique Shock-Turbulent Boundary Layer Interaction," AIAA Paper 2015-2933.
3. Sivasubramanian, J. and Fasel, H., "Numerical Investigation of Shock-induced Laminar Separation Bubble in Supersonic Flows," AIAA Paper 2015-2641.

M.S. Thesis

1. Hainsworth, J. "Experimental Study of Unswept and Swept Oblique Shock-Turbulent Boundary Layer Interactions," MS Thesis, Department of Aerospace and Mechanical Engineering, University of Arizona, 2014.

XIII. Acknowledgements

The project has been primarily supported by AFOSR (FA9550-14-1-0195) under Dr. Ivett Leyva. Jared Hainsworth (M.S. 2014) was supported by the SMART Scholarship for Service. Additional support has been provided by Raytheon Missile Systems.

XIV. References

[1]Dolling, D. S., "Fifty Years of Shock-Wave/Boundary-Layer Interaction Research: What Next?," *AIAA Journal*, Vol. 39, No. 8, 2001, pp. 1517-1531.

[2]Dussauge, J.-P., Dupont, P. and Debieve, J.-F., "Unsteadiness in Shock Wave Boundary Layer Interactions with Separation," *Aerospace Science and Technology*, Vol. 10, No. 2, 2006, pp. 85-91.

[3]Ganapathisubramani, B., Clemens, N. and Dolling, D., "Low-frequency Dynamics of Shock-Induced Separation in a Compression Ramp Interaction," *Journal of Fluid Mechanics*, Vol. 636, 2009, pp. 397-425.

[4]Ganapathisubramani, B., Clemens, N. T. and Dolling, D. S., "Effects of Upstream Boundary Layer on the Unsteadiness of Shock-Induced Separation," *Journal of Fluid Mechanics*, Vol. 585, 2007, pp. 369-394.

[5]Humble, R., Elsinga, G., Scarano, F. and Oudheusden, B. v., "Three-Dimensional Instantaneous Structure of a Shock Wave/Turbulent Boundary Layer Interaction," *Journal of Fluid Mechanics*, Vol. 622, 2009, pp. 33-62.

[6]Humble, R., Scarano, R. and Oudheusen, B. v., "Unsteady Aspects of an Incident Shock Wave/Turbulent Boundary Layer Interaction," *Journal of Fluid Mechanics*, Vol. 635, 2009, pp. 47-74.

[7]Plotkin, K. J., "Shock Wave Oscillation Drive by Turbulent Boundary Layer Fluctuations," *AIAA Journal*, Vol. 13, No. 8, 1975, pp. 1036-40.

[8]Poggie, J. and Smits, A., "Shock unsteadiness in a reattaching shear layer," *Journal of Fluid Mechanics*, Vol. 429, 2001, pp. 155-185.

[9]Poggie, J. and Smits, A., "Experimental evidence for Plotkin model of shock unsteadiness in separated flow," *Physics of Fluids*, Vol. 17, 2005, pp.

[10]Touber, E. and Sandham, N., "Low-order stochastic modelling of low-frequency motions in reflected shock-wave/boundary-layer interactions," *Journal of Fluid Mechanics*, Vol. 671, 2011, pp. 417-465.

[11]Grilli, M., Schmid, P. J., Hickel, S. and Adams, N. A., "Analysis of unsteady behaviour in shockwave turbulent boundary layer interaction," *Journal of Fluid Mechanics*, Vol. 700, 2012, pp. 16-28.
[12]Piponniau, S., Dussauge, J., Devieve, J. and Dupont, P., "A Simple Model for Low-Frequency Unsteadiness in Shock-Induced Separation," *Journal of Fluid Mechanics*, Vol. 629, 2009, pp. 87-108.
[13]Pirozzolia, S. and Grassob, F., "Direct numerical simulation of impinging shock wave/turbulent boundary layer interaction at M=2.25," *Physics of Fluids*, Vol. 18, 2006, pp. 1-17.
[14]Touber, E. and Sandham, N., "Large-eddy simulation of low-frequency unsteadiness in a turbulent shock-induced separation bubble," *Theoretical and Computational Fluid Dynamics*, Vol. 23, No. 2, 2009, pp. 79-107.
[15]Clemens, N. T. and Narayanaswamy, V., "Low-Frequency Unsteadiness of Shock Wave/Turbulent Boundary Layer Interactions," *Annual Review of Fluid Mechanics*, Vol. 46, No. 1, 2014, pp. 469-492.
[16]Robinet, J.-C., "Bifucations in Shock-Wave/Laminar-Boundary-Layer Interaction: Global Instability Approach," *Journal of Fluid Mechanics*, Vol. 579, 2007, pp. 85-112.
[17]Pagella, A., Rist, U. and Wagner, S., "Numerical Investigations of Small–amplitude Disturbances in a Boundary Layer with Impinging Shock Wave at Ma = 4.8," *Physics of Fluids*, Vol. 14, 2002, pp. 2088-2101.
[18]Pagella, A., Babucke, A. and Rist, U., "Two–dimensional Numerical Investigations of Small–amplitude Disturbances in a Boundary Layer at Ma = 4.8: Compression Corner versus Impinging Shock Wave," *Physics of Fluids*, Vol. 2004, 2004, pp. 2272–2281.
[19]Erengil, M. E. and Dolling, D. S., "Effects of Sweepback on Unsteady Separation in Mach 5 Compression Ramp Interactions," *AIAA Journal*, Vol. 31, No. 2, 1993, pp. 302-11.
[20]Schmisseur, J. D. and Dolling, D. S., "Fluctuating Wall Pressures Near Separation in Highly Swept Turbulent Interactions," *AIAA Journal*, Vol. 32, No. 6, 1994, pp. 1151-1157.
[21]Smits, A. and Dussauge, J."Turbulent Shear Layers in Supersonic Flow," *Springer, New York*,editted by
[22]Settles, G. S. and Kimmel, R. L., "Similarity of Quasiconical Shock Wave/Turbulent boundary-Layer Interactions," *AIAA Journal*, Vol. 24, No. 1, 1986, pp. 47-53.
[23]Settles, G. and Dolling, D."Swept shock wave boundary layer interaction," *AIAA Progress Series: Volume on Tactical Missile Aerodynamics*,editted by
[24]Settles, G. and Teng, H., "Cylindrical and Conical Upstream Influence Regims of Three-Dimensional Shock/Turbulent Boundary Layer Interactions," *AIAA Journal*, Vol. 24, 1984, pp. 47-53.
[25]Horstman, C., "A computational study of complex three-dimensional compressible turbulent flowfields," *AIAA Journal*, Vol. 23, No. 10, 1985, pp. 1461-1462.
[26]Holden, M."Experimental Studies of Quasi-Two-Dimensional and Three-Dimensional Viscous Interaction Regions Induced by Skewed-Shock and Swept-Shock Boundary Layer Interactions,"*AFOSR Technical Report 84-1228*,editted by
[27]Dawson-Ruiz, R., Pederson, C. and Little, J., "Effects of Sweep on Impinging Oblique Shock-Turbulent Boundary Layer Interaction," *AIAA Paper*, 2015-2933, 2015.
[28]Souverein, L. J., Dupont, P., Debiève, J.-F., Dussauge, J.-P., Oudheusden, B. V. v. and Scarano, F., "Effect of Interaction Strength on Unsteadiness in Turbulent Shock-Wave-Induced Separations," *AIAA Journal*, Vol. 48, No. 7, 2010, pp. 1480-1493.
[29]Webb, N., Clifford, C. and Samimy, M., "Control of oblique shock wave/boundary layer interactions using plasma actuators," *Experiments in Fluids*, Vol. 54, No. 6, 2013, pp. 1-13.
[30]Maise, G. and McDonald, H., "Mixing Length and Kinematic Eddy Viscosity in a Compressible Boundary Layer," *AIAA Journal*, Vol. 6, No. 1, 1968, pp. 73-80.
[31]Hainsworth, J., Dawson, R. and Little, J., "Experimental Study of Unswept and Swept Oblique Shock-Turbulent Boundary Layer Interactions," AIAA Paper 2014-2738, 2014.
[32]Klomparens, R., Gamba, M. and Driscoll, J., "Boundary Layer Separation in a 3D Shock Train," AIAA Paper 2015-1519 2015.
[33]Hakkinen, R., Greber, I., Trilling, L. and Abarbanel, S."The Interaction of an Oblique Shock Wave with a Laminar Boundary Layer,"*NASA Technical Report 2-18-59W*,editted by

[34]van Leer, B., "Flux-Vector Splitting for the Euler Equations," *International Conference on Numerical Methods in Fluid Dynamics*, 170 1982.
[35]Zhong, X., "High-Order Finite-Difference Schemes for Numerical Simulation of Hypersonic Boundary-Layer Transition," *Journal of Computaitonal Physics*, Vol. 144, 1998, pp. 662-709.
[36]Laible, A., Mayer, C. and Fasel, H., "Numerical Investigation of Transition for a Cone at Mach 3.5: Oblique Breakdown," AIAA Paper 2009-3557 2009.
[37]Laible, A., Mayer, C. and Fasel, H., "Numerical Investigation of Supersonic Transition for a Circular Cone at Mach 3.5," AIAA Paper 2008-4397 2008.
[38]Poinsot, T. and Lele, S., "Boundary Conditions for Direct Simulations of Compressible Viscous Flows," *Journal of Computaitonal Physics*, Vol. 101, 1992, pp. 104-129.
[39]Harris, P. J."Numerical Investigation of Transitional Compressible Plane Wakes,"*Ph.D. Dissertation, Aeropace and Mechanical Engineering, The University of Arizona*,editted by
[40]Katzer, E., "On the Length scales of Laminar Shock/boundary-layer Interaction," *Journal of Fluid Mechanics*, Vol. 206, 1989, pp. 477-496.
[41]Sansica, A., Sandham, N. and Hu, Z., "Stability and Unsteadiness in a 2D Laminar Shock-Induced Separation Bubble," *AIAA*, 2014-2982 2013.
[42]Sansica, A., Sandham, N. and Hu, Z., "Forced Response of a Laminar Shock-induced Separation Bubble," *Phys. Fluids*, Vol. 26, 2014, pp.
[43]Sivasubramanian, J. and Fasel, H., "Numerical Investigation of Shock-Induced Laminar Separation Bubble in a Mach 2 Boundary Layer," AIAA Paper 2015-2641 2015.
[44]Sivasubramanian, J. and Fasel, H., "Numerical Investigation of the Development of Three-dimensional Wavepackets in a Sharp Cone Boundary Layer at Mach 6," *Journal of Fluid Mechanics*, Vol. 756, 2014, pp. 600-649.
[45]Salemi, L. and Fasel, H., "Linearized Navier-Stokes Simulation of the Spatial Stability of a Hypersonic Boundary Layer in Chemical Equilibrium," AIAA Paper 2014-2984 2013.
[46]Sandham, N., Schuelein, E., Wagner, A., Willems, S. and Steelant, J., "Transitional Shock-wave/boundary-layer Interactions in Hypersonic Flow," *Journal Fluid Mechanics*, Vol. 752, 2014, pp. 349-382.

1.

1. Report Type

Final Report

Primary Contact E-mail
Contact email if there is a problem with the report.

jesselittle@email.arizona.edu

Primary Contact Phone Number
Contact phone number if there is a problem with the report

520-626-8677

Organization / Institution name

University of Arizona

Grant/Contract Title
The full title of the funded effort.

Investigation of 3D Shock-Boundary Layer Interaction: A Combined Approach using Experiments, Numerical Simulations and Stability Analysis

Grant/Contract Number
AFOSR assigned control number. It must begin with "FA9550" or "F49620" or "FA2386".

FA9550-14-1-0195

Principal Investigator Name
The full name of the principal investigator on the grant or contract.

Jesse Little

Program Manager
The AFOSR Program Manager currently assigned to the award

Ivett Leyva

Reporting Period Start Date

07/15/2014

Reporting Period End Date

07/14/2015

Abstract

The characteristics of unswept and swept impinging oblique shock turbulent boundary layer interaction (SBLI) are examined using experiments, simulations and stability analysis. The experimental focus is on application of stereoscopic particle image velocimetry (PIV) to the flow field produced by an impinging shock (produced by a 15 degree wedge) that is swept at angles of 0, 22.5, and 40 degrees in Mach 2.3 flow. The SBLI is investigated at three spanwise planes. The interaction length is found to decrease with increasing sweep angle across the test matrix. The 22.5 degree and unswept case have cylindrical similarity and the 40 degree interaction appears conical. The present study also includes a mirrored 40 degree swept case, which shows that the results are not due to a particular sidewall boundary layer. All cases show separated flow in the interaction region and most contain reverse flow that is clearly outside of the measurement uncertainty. A corresponding numerical SBLI study is undertaken for a laminar approach boundary layer at Mach 2.0. The numerical conditions are chosen for modification and validation of an existing in-house code. The skin friction and pressure distribution from the simulations are compared to experimental measurements and numerical results available in the literature. Results confirm the asymmetric nature of the separation bubble as reported in the classical literature. In addition to the steady flow field calculations, the response to low–amplitude disturbances is investigated in order to study the

linear stability behavior of the separation bubble. For comparison, both the development of two–dimensional and three–dimensional (oblique) disturbances are studied with and without the impinging oblique shock. Furthermore, the effects of the shock incidence angle and Reynolds number are investigated. Three–dimensional direct numerical simulations are performed in order to explore the laminar-turbulent transition process in the presence of a laminar separation bubble generated by an impinging shock. The results presented here summarize efforts during a one-year seed grant and show that the necessary tools for linking experiments and computations have been developed. A major focus of future efforts is to more closely link the research tracks.

Distribution Statement

This is block 12 on the SF298 form.

Distribution A - Approved for Public Release

Explanation for Distribution Statement

If this is not approved for public release, please provide a short explanation. E.g., contains proprietary information.

SF298 Form

Please attach your SF298 form. A blank SF298 can be found here. Please do not password protect or secure the PDF The maximum file size for an SF298 is 50MB.

Little-SF298.pdf

Upload the Report Document. File must be a PDF. Please do not password protect or secure the PDF . The maximum file size for the Report Document is 50MB.

Little_AFOSR_Final_Report.pdf

Upload a Report Document, if any. The maximum file size for the Report Document is 50MB.

Archival Publications (published) during reporting period:

Changes in research objectives (if any):

Change in AFOSR Program Manager, if any:

Extensions granted or milestones slipped, if any:

AFOSR LRIR Number

LRIR Title

Reporting Period

Laboratory Task Manager

Program Officer

Research Objectives

Technical Summary

Funding Summary by Cost Category (by FY, $K)

	Starting FY	FY+1	FY+2
Salary			
Equipment/Facilities			
Supplies			
Total			

Report Document

Report Document - Text Analysis

Report Document - Text Analysis

Appendix Documents

2. Thank You

E-mail user

Nov 23, 2015 01:19:18 Success: Email Sent to: jesselittle@email.arizona.edu